

DETECTION AND IDENTIFICATION OF DELAMINATION DEFECTS IN CFRP LAMINATES USING NON-LINEAR FREQUENCY-MODULATED INFRARED THERMAL WAVE TESTING TECHNOLOGY

by

Qing-Ju TANG^{a*}, Cui-Zhu FENG, Zhi-Bo WANG, and Hao-Dong LI

^a School of Mechanical Engineering,
Heilongjiang University of Science and Technology, Harbin, China

Original scientific paper
<https://doi.org/10.2298/TSCI230610035T>

In the process of preparation and service, the carbon fiber reinforced polymer (CFRP) material is prone to defects such as delamination and inclusions, which seriously impact the normal use. In this paper, non-linear frequency-modulated (the logarithmic sweep) thermal excitation is used to carry out finite element simulation and experimental research. In order to investigate how different detection process parameters affect defects, the impact of different detection parameters on the surface temperature difference and contrast is analyzed, and the detection parameters that can quickly identify defects and have better recognition effect are obtained.

Key words: CFRP laminates, non-linear frequency-modulated, detection parameters

Introduction

Carbon fiber reinforced composite material is a laminate formed by carbon fiber layer cloth after heat curing with epoxy resin. The features of it include high specific strength, resistance to corrosion, and resistance to tiredness [1]. It is widely used in aerospace (aircraft doors, brakes, fuselage, etc.), transportation (automobile body), medical treatment (used as orthopedic implants or prostheses) [2] and other fields. It is simple to create interlayer delamination (up to 50%), cracks, inclusions, and other flaws during the real use process. In order to avoid potential safety hazards, using infrared non-destructive testing technology, the purpose of detecting defects can be achieved without damaging the detected objects.

Study on the theory and simulation of non-linear frequency modulated (the logarithmic sweep) infrared thermal wave

Homogenization of dissimilar materials

In order to reduce the computational load and running memory in the simulation process and improve the modelling efficiency. In this paper, the homogeneous material model is used to simulate the cross-ply carbon fiber composite material as shown in fig. 1. The equal calibration physical parameters, tab. 1, can be directly calculated by the mixing rule [3]:

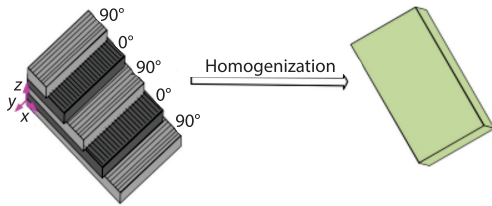
$$\rho = X_n \rho_n + X_s \rho_s, \quad c = X_n c_n + X_s c_s \quad (1)$$

where X_n is the volume fraction of carbon fiber, X_s – the volume fraction of resin, ρ_n – the density of carbon fiber, ρ_s – the density of resin, c_n – the specific heat capacity of carbon fiber, and c_s – the specific heat capacity of resin.

* Corresponding author, e-mail: tangqingju@126.com

Table 1. Thermophysical parameters of CFRP laminates [4-6]

Materials	Volume fraction	Density	Specific heat capacity	Thermal conductivity
Carbon fiber	0.6	1760	777	$k_{n,x}=10.5, k_{n,z}=2$
Resin	0.4	1200	1210	0.2
CFRP laminates	1	1536	950	$k_{xx}=k_{yy}=3.908, k_{zz}=0.43$

**Figure 1. Homogenization of heterogeneous composite materials**

In view of the anisotropy of the thermal conductivity of carbon fiber materials' thermal conductivity, the thermal conductivity in the x -, y -, and z -directions should be calculated according to the different distribution of carbon fibers:

$$\frac{1}{k_{zz}} = \frac{X_n}{k_{n,z}} + \frac{X_s}{k_s}, \quad k_{xx} = X_n k_{n,x} + X_s k_s, \quad k_{xx} = k_{yy} \quad (2)$$

where k_{xx} , k_{yy} , and k_{zz} are the thermal conductivity of the CFRP laminate in the main direction in the global co-ordinate system.

Establish a model of 3-D heat transmission

If the temperature of the i layer CFRP laminate is $T_i = T_i(x, y, z, t)$, the 3-D heat conduction model of the CFRP laminate can be obtained according to the basic law of Fourier heat transfer. The model of 3-D heat transmission [7]:

$$k_{ixx} \frac{\partial^2 T_i}{\partial x^2} + k_{iyy} \frac{\partial^2 T_i}{\partial y^2} + k_{izz} \frac{\partial^2 T_i}{\partial z^2} + 2k_{ixy} \frac{\partial^2 T_i}{\partial x \partial y} = \rho c \frac{\partial T_i}{\partial t}, \quad i = 1, 2, 3 \dots \quad (3)$$

where k_{ixx} , k_{iyy} , and k_{izz} are the thermal conductivity in the i^{th} layer's global co-ordinate system's main direction, respectively.

In a single cycle, the heat flux density distribution loaded on the excitation surface M [8]:

$$q(t) = q_{SC} + q_{DC} = \frac{q_{\max}}{2} \left\{ 1 + \cos \left[2\pi \frac{Tf_s}{\ln \left(\frac{f_e}{f_s} \right)} \left(\left(\frac{f_e}{f_s} \right)^{t/T} - 1 \right) \right] \right\}, \quad t \in [0, T] \quad (4)$$

Initial conditions and boundary conditions read:

$$T(x, y, z, t)|_{t=0} = T(x, y, z, 0) = T_{\text{envi}} \quad (5)$$

$$q|_{\Lambda} = h[T_{\text{envi}} - T(x, y, z, t)] + \varepsilon\sigma[T_{\text{envi}}^4 - T(x, y, z, t)^4] \quad (6)$$

$$q|_{M=M_s} = h[T_{\text{envi}} - T(x, y, z, t)] + \varepsilon\sigma[T_{\text{envi}}^4 - T(x, y, z, t)^4] \quad (7)$$

Establishment of finite element simulation

The flat-topped blind hole is used to simulate the delamination defects of CFRP. The diameter and depth of the defects are shown in fig. 2(a). The defect depths, H , in the first to fifth columns are 0.4 mm, 0.6 mm, 0.8 mm, 1.0 mm, and 1.2 mm, respectively. The defect diameters, D , in the first to fifth rows are 10 mm, 8 mm, 6 mm, 4 mm, and 2 mm, respectively. According

to the thermophysical parameters of CFRP, logarithmically modulated non-linear frequency modulation (NLFM) thermal excitation is applied to the simulation model's upper surface.

Figure 3 shows the simulated temperature heat maps at different times obtained under the conditions of initial frequency of 0.2 Hz, termination frequency of 0.05 Hz, scanning period of 20 seconds and excitation power of 2000 W. It can be seen from fig. 3 that at 1.5 seconds, the specimen begins to be excited by heat, and the defects in columns 1-3 begin to appear. When the excitation lasts for 8 seconds, the defects are basically displayed completely. The defect contour is relatively clear. At 17.5 seconds, the heat conduction speed inside the laminate is slower, and the heat dissipation speed is slow, resulting in heat accumulation and blurred edge of the defect.

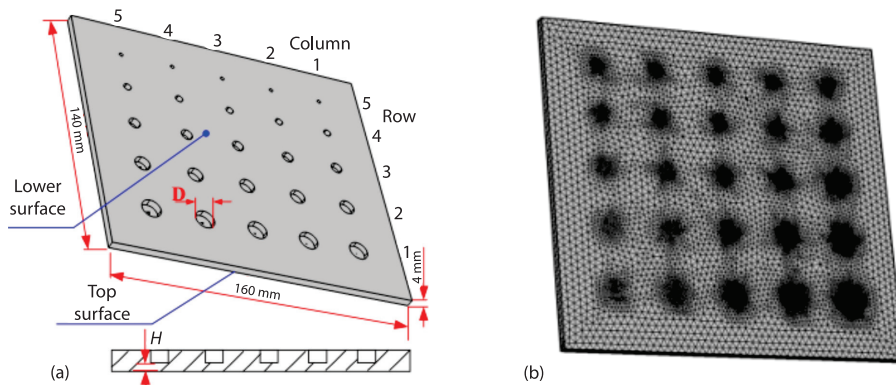


Figure 2. Finite element simulation diagram;
(a) CFRP laminate structure and (b) finite element ultra-fine meshing diagram

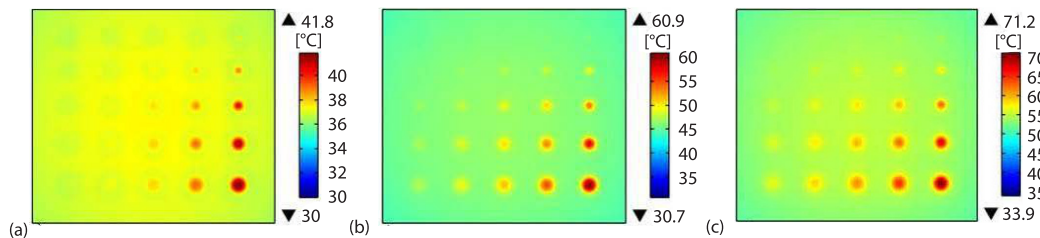


Figure 3. Simulation heat map at different times; (a) 1.5 seconds, (b) 8 seconds, and (c) 17.5 seconds

Detection of process parameters

Different initial frequencies: As seen in fig. 4(a), the larger the initial frequency, the more the number of wave peaks in the temperature difference curve, and the more frequent the waveform rises and falls, which is not conducive to the detection of defects.

Different termination frequencies: As shown in fig. 4(b), the larger the termination frequency, the larger the fluctuation of the thermal wave rise and fall, the shorter the heating time, which is not conducive to the detection of defects.

Different scanning periods: The outcomes are displayed in fig. 4(c). The difference between the comparison values of the scanning period is 10 seconds, and the thermal waves within the minimum period of 20 seconds in the four groups of cycles are intercepted, respectively. It is found that the number of wave peaks is basically the same, but the temperature difference obtained by the smaller scanning period is higher, which is more conducive to defect detection.

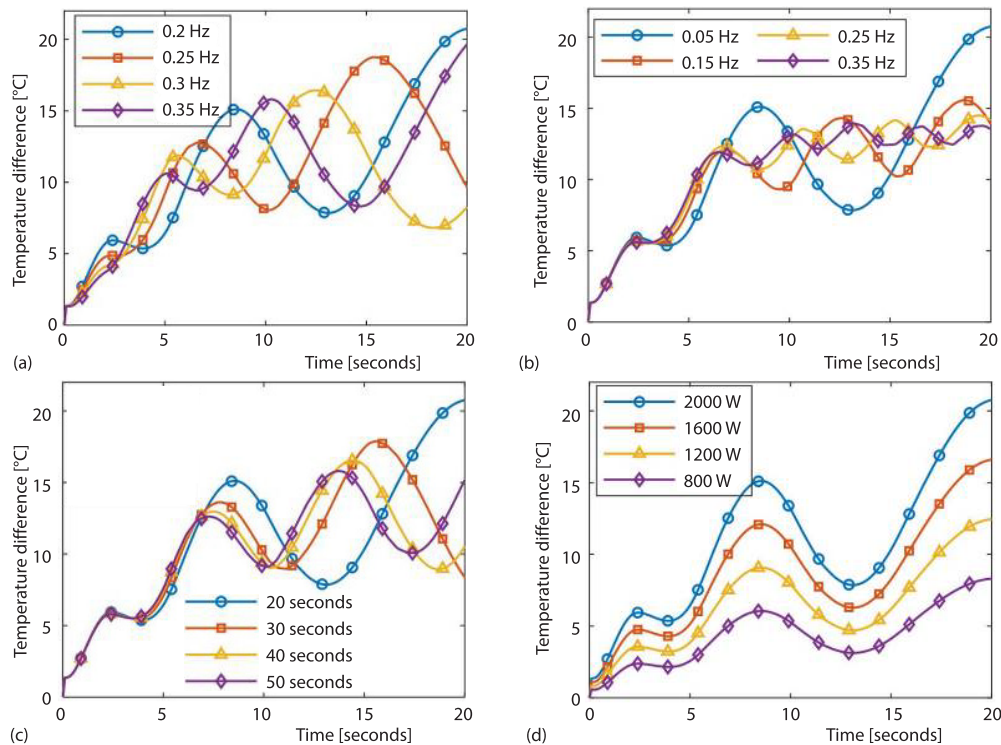


Figure 4. The effect of varied detection parameters on the surface temperature differential in the simulation; (a) initial frequency, (b) termination frequency, (c) scanning cycle, and (d) excitation power

Different excitation power: As shown in fig. 4(d), the surface temperature difference under the excitation power of 2000 W, 1600 W, 1200 W, and 800 W decreases successively. Under the condition that the specimen material allows, the larger excitation power is more conducive to defect detection.

Experimental study

The NLFM experimental detection system is mainly composed of NLFM thermal excitation system (halogen lamp, dimmer, NI USB-6259 BNC data acquisition card, LabVIEW software), image sequence acquisition system (FLIR A655SC infrared thermal imager), image sequence analysis and processing system (thermal imager, FLIR ResearchIR Max software, *etc.*).

Under the same detection process parameters, as shown in figs. 5(a), and 5(b), the smaller the initial and termination frequencies, the fewer the number of wave peaks in the temperature difference curve. The change of rising and falling in the thermal wave is slow, the heating time is relatively long, which is beneficial to the rapid identification of defects, and the detection effect is good. As illustrated in fig. 5(c), the number of peaks of surface temperature difference in different scanning periods (difference of 10 seconds) within the minimum period of 20 seconds is basically the same, but the temperature difference obtained by the smaller scanning period is higher, which is more conducive to defect detection. As shown in fig. 5(d), the surface temperature difference curve trend is basically the same, the temperature difference

value is different, and the higher power surface temperature difference is larger. In the case of specimen material permission. Try to choose a larger excitation power to detect defects.

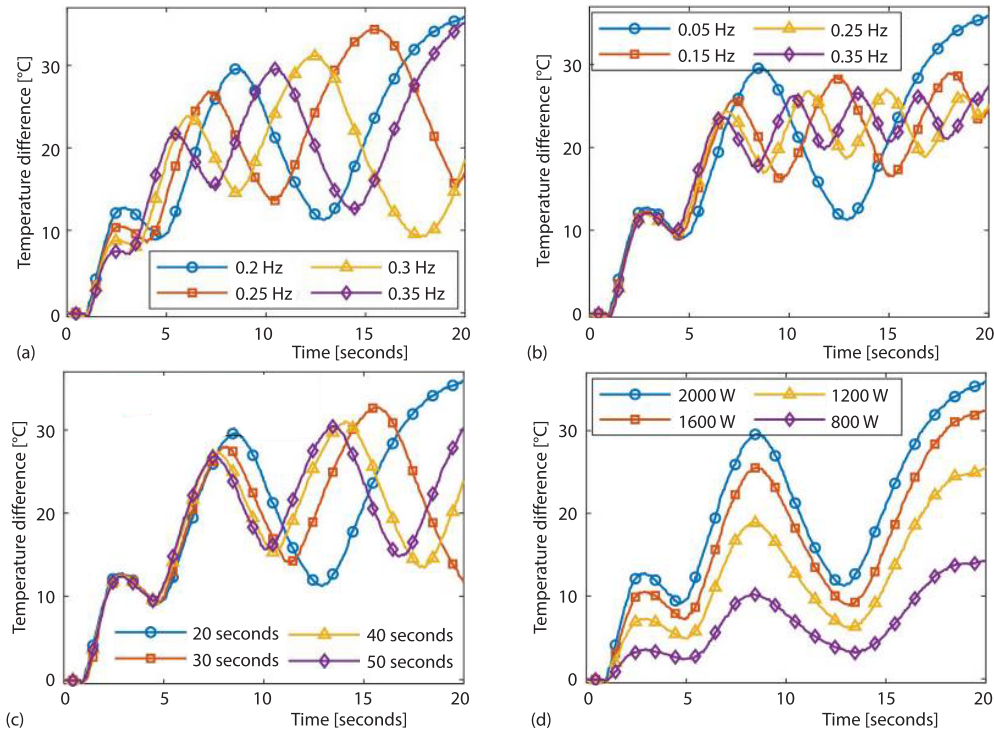


Figure 5. The effect of varied detection parameters on the surface temperature differential during the experiment; (a) initial frequency, (b) termination frequency, (c) scanning cycle, and (d) excitation power

Simulation experiment data comparison

In light of the aforementioned analysis's findings, the detection parameters with the best defect detection effect are adopted: the initial frequency is 0.2 Hz, the termination frequency is 0.05 Hz, the scanning period is 20 seconds, and the excitation power is 2000 W. The change of surface temperature difference during the experiment and simulation process is compared, figs. 6 and 7.

The results show that the surface temperature trends of simulation and experiment are basically the same. A greater diameter corresponds to a greater surface temperature differential when the defect depth is 0.4 mm. When the defect diameter is 10 mm, the shallower the buried depth is, the larger the surface temperature difference is. However, there is a certain gap between the simulation and the experiment in the temperature difference value. The reasons are given:

- The simulation is ideal and the environment is controllable. The experiment is greatly affected by the surrounding environment.
- The accuracy of the experimental equipment and the infrared radiation of the equipment itself affect the identification of the defect characteristics.
- The model in the simulation has been homogenized, but the internal structure of the material in the experiment is more complex.

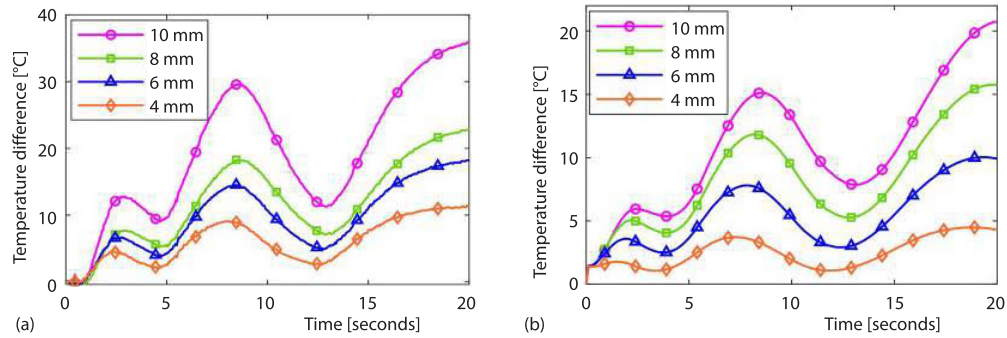


Figure 6. Comparison of simulation and experimental results of different diameter defects; (a) experimental figure and (b) simulation figure

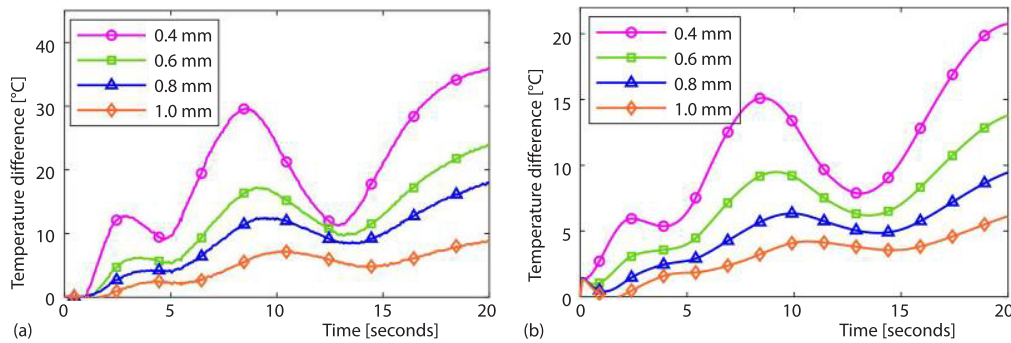


Figure 7. Comparison of simulation and experimental results of defects at different depths; (a) experimental figure and (b) simulation figure

Conclusion

In this paper, the NLFM of logarithmic modulation was considered. A 3-D model for heat transmission is created after homogenization treatment of the specimen, and the impact of different detection parameters on the surface temperature differential of CFRP laminates are examined. The results show that under the premise of not affecting the material properties of the specimen, the selection of smaller initial and termination frequencies, scanning cycles, and larger excitation power is more conducive to the detection of defects.

Acknowledgment

This project is supported by Natural Science Foundation of Heilongjiang Province (Grant No. JQ2023E011).

Nomenclature

D – defect diameter, [mm]
 c – specific heat capacity, [$\text{Jkg}^{-1}\text{°C}$]
 H – defect depth, [mm]

Greek symbol
 ρ – density of CFRP laminates, [kgm^{-3}]

References

- [1] Xu, C., Zuhao, W., Research Progress in Numerical Simulation of Mechanical Properties of CFRP Laminates (in Chinese), *Aviation Manufacturing Technology*, 66 (2023), 15, pp. 60-70
- [2] Sikui, C., Ronghui, G., Application and Prospect of Carbon Fiber Reinforced Resin Matrix Composites (in Chinese), *Journal of Textile Science and Engineering*, 40 (2023), 4, pp. 102-122

- [3] Hebing, X., Experimental Study and Numerical Simulation of Short Pulse Laser Milling of Woven Carbon Fiber Composites (in Chinese), Ph. D. Thesis, Shanghai Jiaotong University, Shanghai, China, 2017
- [4] El-Hage, Y, *et al.*, Thermal Conductivity of Textile Reinforcements for Composites, *Journal of Textiles and Fibrous Materials*, 1 (2018), ID2515221117751154
- [5] Villiere, M, *et al.*, Experimental Determination and Modelling of Thermal Conductivity Tensor of Carbon/Epoxy Composite, *Composites Part A*, 46 (2013), 3, pp. 60-68
- [6] Zhang, H, *et al.*, Experimental Study of the Anisotropic Thermal Conductivity of 2-D Carbon-Fiber/Epoxy Woven Composites, *Composite Structures*, 267 (2021), 1, ID113870
- [7] Jinlong, G., Research on Infrared Thermal Wave Radar Imaging Detection Technology for CFRP Laminate Defects and Ply Orientation (in Chinese), Ph. D. Thesis, Harbin University of Technology, Harbin, China, 2016
- [8] Saaid, H., *et al.*, On the Application of an Optimized Frequency-phase Modulated Waveform for Enhanced Infrared Thermal Wave Radar Imaging of Composites, *Optics and Lasers in Engineering*, 137 (2021), ID106411